Journal of Alloys and Compounds 753 (2018) 636–641

Contents lists available at ScienceDirect

Journal of Alloys and Compounds

journal homepage: http://www.elsevier.com/locate/jalcom

Structural and bonding transformation of $Al_{0.67}CrCoCuFeNi$ high-entropy alloys during quenching

Kun Zhang [a, b], Shaopeng Pan [c], Weiqi Tang [a, b], Yating Zhang [a, b], Bingchen Wei [a, b, *]

[a] Key Laboratory of Microgravity (National Microgravity Laboratory), Institute of Mechanics, Chinese Academy of Sciences, Beijing 100190, China
[b] School of Engineering Science, University of Chinese Academy of Sciences, Beijing 101408, China
[c] College of Materials Science and Engineering, Taiyuan University of Technology, Taiyuan, 030024, China

ARTICLE INFO

Article history:
Received 12 February 2018
Received in revised form
18 April 2018
Accepted 21 April 2018
Available online 23 April 2018

Keywords:
High-entropy alloys
Phase transformation
Bonding characteristic

ABSTRACT

Structural and bonding transformation of the $Al_{0.67}CrCoFeNi$ high-entropy alloys (HEA) during quenching is investigated by molecular dynamics simulations. At a high cooling rate, some short-ranged ordered clusters, such as FCC, HCP and BCC crystalline clusters are already present in the almost amorphous HEAs. When the cooling rate decreases, the atoms become packed more orderly and ultimately form a nano-polycrystalline structure dominated by FCC structures. The BCC structures appear only as an intermediate state acting on the course of crystallization, while the HCP structure can be viewed as the precursor of the malposed FCC structure due to the identical first neighbor distances. In liquid HEAs, the low-symmetry and low-coordination bond pairs, either transform to high-symmetry and high-coordination 1551 bond pairs, or transform to 1(5,4)41 bond pairs for FCC structure and 1661 bond pairs for an HCP structure, depending on the cooling rates. This study will contribute to a better understanding of the essential phase change in HEAs.

1. Introduction

High entropy alloys (HEAs) have attracted considerable research interests due to their high strength, ductility, toughness and corrosion resistance compared with traditional alloys [1–4]. The solidified structure of HEAs is generally simple, even though they are comprised of five or more than five elements. Their simple crystal lattices exhibit both the individual characteristics of their constituents and collective features. Nowadays, HEAs have been shown to have a wide application prospect in various fields, such as in the aerospace industry or in the fabrication of tool and damage resistant materials [5–8]. In earlier work on HEAs, numerous studies focused on the study of single-phase HEAs. Indeed, most of the described HEAs contained multiple phases instead of a single solid-solution phase [1,9]. The formation of multiphases in HEAs is strongly associated with the local atomic stress/strain environment, thermal-equilibrium behavior, and interatomic interactions among the constituent elements [10,11]. Understanding the underlying thermodynamic characteristic of HEAs through integrated experiments and thermodynamic modeling can provide an insight into the design of multiphase HEAs [12]. Especially, with little Al addition, CrCoCuFeNi HEAs are composed of a simple FCC solid-solution structure. As the Al content reaches $x = 0.8$, a BCC structure appears, which consisted of mixed FCC and BCC eutectic phases [13]. It is believed that excessive Al is capable of triggering diffusive transformations from a molten to a crystalline phase via an intermediate amorphous structure [14]. However, the basic understanding of the structural stability and transformation properties is still lacking, due to the complicated elemental diffusion and atomic-bonding environments [11,14]. Recently, transformation-induced plasticity has been successfully employed in HEAs to overcome the strength-ductility trade-off [15,16]. In addition, altering the cooling conditions is another effective pathway to achieve multiphase structures. Nevertheless, how the HEA liquid changes into the solid as well as the evolution of intermediate states during a rapid quenching process need to be further investigated. In addition, the relation between the structural transformation and bonding characteristic should also be elucidated.

First principle simulation based on the density functional theory is useful to investigate the physical and structural property of HEAs [17–19]. Such calculations can provide accurate descriptions of the

* Corresponding author. Key Laboratory of Microgravity (National Microgravity Laboratory), Institute of Mechanics, Chinese Academy of Sciences, Beijing 100190, China.
E-mail address: weibc@imech.ac.cn (B. Wei).

https://doi.org/10.1016/j.jallcom.2018.04.252
0925-8388/

binding energies and bonding characteristic among the atoms. However, the technique is limited to a small number of atoms. Motivated by the above concerns, in this work, the classical molecular dynamics (MD) simulation is used to examine the bonding characteristic and origins of the structural transformation in $Al_{0.67}$CrCoFeNi HEAs. A possible nucleation mechanism in liquid HEAs is proposed. The findings of this study can pave new paths for guiding the future development of promising single-phase and multiphase HEAs.

2. Simulation details

The highly parallelized Large-scale Atomic/Molecular Massively Parallel Simulator (LAMMPS) MD simulation package [20] is employed for computations, while the visual analysis and post-processing of molecular trajectories are performed with the open visualization tool (OVITO) [21]. The simulations are conducted using the classical Lenard-Jones (LJ) pair-potentials with parameters obtained from the literature [14]. These LJ force-field parameters have been found to agree well with previous results, where a maximum deviation of ~11% is observed [22–24]. An FCC lattice of 9.2 nm × 9.2 nm × 9.2 nm composed of randomly distributed Al, Co, Cr, Cu, Fe and Ni atoms, as shown in Fig. 1, is constructed. The cuboidal simulation cell contains 37,044 atoms with periodic boundary conditions imposed in all the directions. First, the energy minimization of the structure is performed using the steepest descent algorithm with an energy tolerance of 10^{-6} and force tolerance of 10^{-8} (eV/Å). Then, this model is initialized at 5300 K under an isothermal-isobaric (NPT) ensemble at zero pressure for 100 ps. Subsequently, the alloy is rapidly quenched to 300 K at different cooling rates (0.05 K/ps; 0.34 K/ps; 0.5 K/ps; 5 K/ps). A time step of 0.001 ps is maintained throughout all our simulations. In order to record the averaging structural information at each given temperature, we create five atomic trajectories using slightly different integration time steps starting from the same initial configuration.

3. Results and discussions

The pair correlation functions (PCF) curves of the $Al_{0.67}$CrCoFeNi HEAs are shown in Fig. 2. It is worth noting that the main peak height of the PCFs, which represents the nearest-neighbor shell, increases significantly with the decrease of the temperature, and the second peak begins to split. At the cooling rates of Q = 5 K/ps and 0.5 K/ps, the second peak begins to split into two subpeaks at 300 K, where the ordered structure in the short range appears. With the decrease of the cooling rate to Q = 0.34 K/ps, the splitting occurs at 1300 K. Additionally, a small shoulder peak between the first and second peaks arises on the left, which indicates that the length of the ordered structure is further extended to a large scale. At the cooling rate of Q = 0.05 K/ps, the left shoulder peak becomes more prominent than the subpeak at the right, suggesting that the orientation of crystalline structures becomes more consistent. The results indicate that the shoulder peak at the left side of the second peak is due to the appearance of short- or medium-range ordered structures [25].

To achieve a better characterization of the internal structural evolution, common neighbor analysis (CNA) is implemented to obtain the general characteristic signature by computing the topology of the bonds that connect the surrounding neighbor atoms [26]. The adaptive CNA with variable cut-offs automatically determines the threshold radius for phase identification of the atoms in the multicomponent environment of the HEA lattice. The CNA parameters of the quenched HEAs with different cooling rates are shown in Fig. 3. The detailed fractions of various crystal structures are listed in Table 1. When the cooling rate is Q = 5 K/ps, some short-ranged ordered clusters, such as FCC, HCP and BCC crystalline clusters are already present in the HEAs, which are difficult to observe in experiments due to the resolution limit. The crystallites distribute discretely at random locations, which makes the crystalline clusters seem more stable and compact than their surroundings due to the dense packing. Further reducing the cooling rate (Q = 0.5 and 0.34 K/ps) will aggregate more crystalline clusters which become larger. An evident characteristic is that FCC and HCP structures alternate with each other. Instead, when the cooling rate continues to reduce (Q = 0.05 K/ps), the atoms become packed more orderly and ultimately form a nano-polycrystalline structure dominated by FCC structures. Compared with the conventional alloys, the severely distorted lattice in HEAs may make the atoms more difficult to diffuse. Xue reported that the high-cooling HEAs favored the formation of FCC and BCC phase respectively, rather than the dual-phase structure, due to the cooling rate-related sluggish diffusion effect [27]. It should be emphasized that BCC structures appear only as an intermediate state acting on the course of crystallization, which initially increase from 0.3% to 2.0% when the cooling rate decreases from 5 K/ps to 0.34 K/ps, and eventually

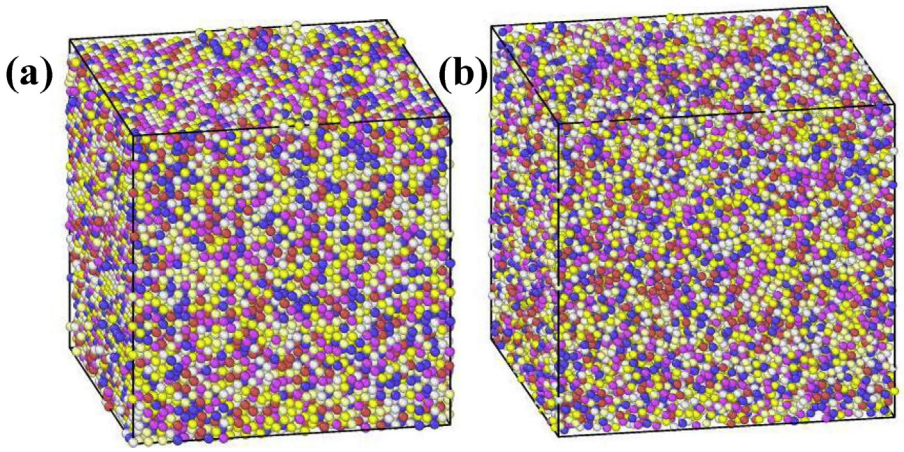

Fig. 1. Elements are randomly distributed in (a) an FCC lattice then (b) kept at 5300 K for 100 ps under a NPT ensemble. The various colors represent the different elements: Al in red, Co in blue, Cr in green, Cr in pale yellow, Cu in white, Fe in yellow, and Ni in purple. (For interpretation of the references to color in this figure legend, the reader is referred to the Web version of this article.)

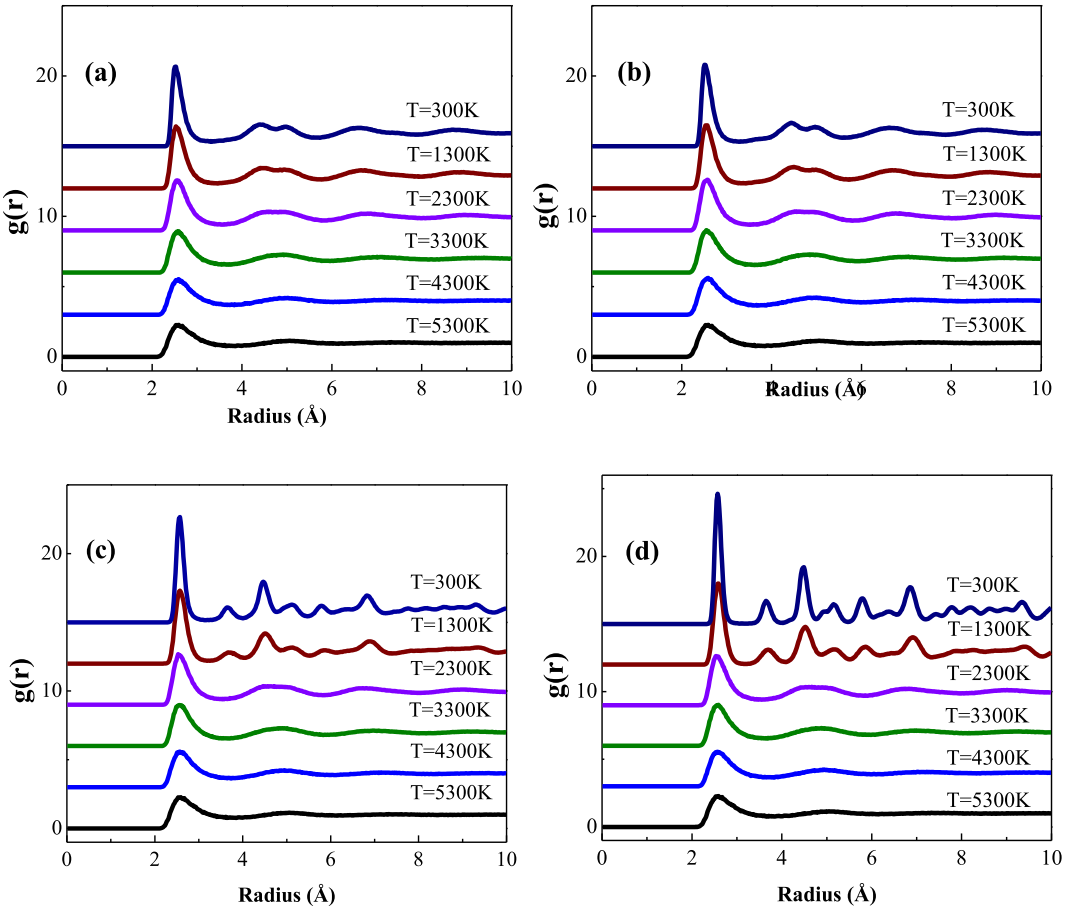

Fig. 2. Pair correlation functions (PCFs) of the $Al_{0.67}CrCoFeNi$ HEAs at different temperatures and different cooling rates (a) 5 K/ps; (b) 0.5 K/ps; (c) 0.34 K/ps; (d) 0.05 K/ps.

decrease to 0.6% with further decrease to 0.05 K/ps.

The bond orientational order parameter is usually used to describe the symmetry of bond orientations regardless of the bond lengths. The structural evolution can be defined according to the distribution of the local bond orientational order parameter Q6 [28,29]. A bond is defined as the vector joining a pair of neighboring atoms. There are two methods to obtain the bond order parameters, one is the "global" average bond order parameter; the other is the "local" bond order parameter of a specified atom according to its nearest neighbors. The changes of the local bond orientational order parameter in the liquid and quenched states are illustrated in Fig. 4. In the liquid state, the distribution of the local Q6 has only one flat peak at Q6 = 0.35. In the quenched state at Q = 5 K/ps and 0.5 K/ps, the flat peak gradually shifts toward higher Q6 = 0.47 due to the appearance of some short-ranged crystalline clusters. The peak becomes more evident with the increase of the FCC structure at Q = 0.34 K/ps. More interestingly, another subpeak at Q6 = 0.6 becomes dominant with the decrease of the cooling rate, which agrees well with the increase of the number of HCP structures.

The bonded pairs index (*H-A*) with four integers (*i, j, k, l*) is also used to analyze the structural evolution of HEAs [30]. The first number *i* in the *H-A* index is defined as the bonding of two given atoms (*i* = 1 for bonded pairs and *i* = 2 for non-bonding atoms); *j* is the number of shared nearest neighbors shared by the two atoms; *k* is the number of bonds among the shared neighbors. The fourth digit *l* is needed in case the first three numbers are the same, but the bond geometries are different. Actually, the relationship between *i* and *j* can reflect the bond-breaking and making characteristic in HEAs during quenching. To analyze the information contained in the bonded pairs further, the bonded pairs are divided into two categories: 'saturated bonded pairs', which is when the shared neighbors connect to form a ring, i.e., when *k* = *j*; otherwise, they are designated as 'unsaturated bonded pairs' [31].

Portraits of *k* along *j* of the HEAs with different states are shown in Fig. 5. The liquid state of the HEAs has three accumulation areas: 1321 bond-types related to the rhombohedral structures, 1431 bond-types related to the tetrahedral structures and 1541 bond-types related to the defected icosahedral configurations. It should be noted that the distribution of bond pairs in liquid HEAs is discrete and widespread. The main bond pairs are the 'unsaturated bonded pairs', which have relatively low symmetry and high configurational entropy. At Q = 5 K/ps and 0.5 K/ps in the almost amorphous states, the saturated 1551 bond pairs increase rapidly along with a slight increase of the 1661 bond pairs, which agrees well with previous results with abundant icosahedral order.

Actually, structural evolution from liquid to solid, will also lead to different change of free volume. As shown in Fig. 5b and c, the fraction of saturated 1551 bonded pair decreases, while other unsaturated bonded pairs slightly increase when the cooling rate decreases from 0.5 K/ps to 5 K/ps, thereby the distribution of H-A bond pairs becomes more and more disperse. This means that the bonding characteristic of the $Al_{0.67}CrCoCuFeNi$ HEAs has been changed from the low-symmetry bond pairs to the high-symmetry bond pairs, accompanied by an increased number of nearest neighbors, which results from the break and re-formation of the atomic bonds [32]. Moreover, the fraction of 1551 bond pair decreases with the decrease of the cooling rate from Q = 5 K/ps to Q = 0.5 K/ps, whereby the 1661 bond pairs become more evident.

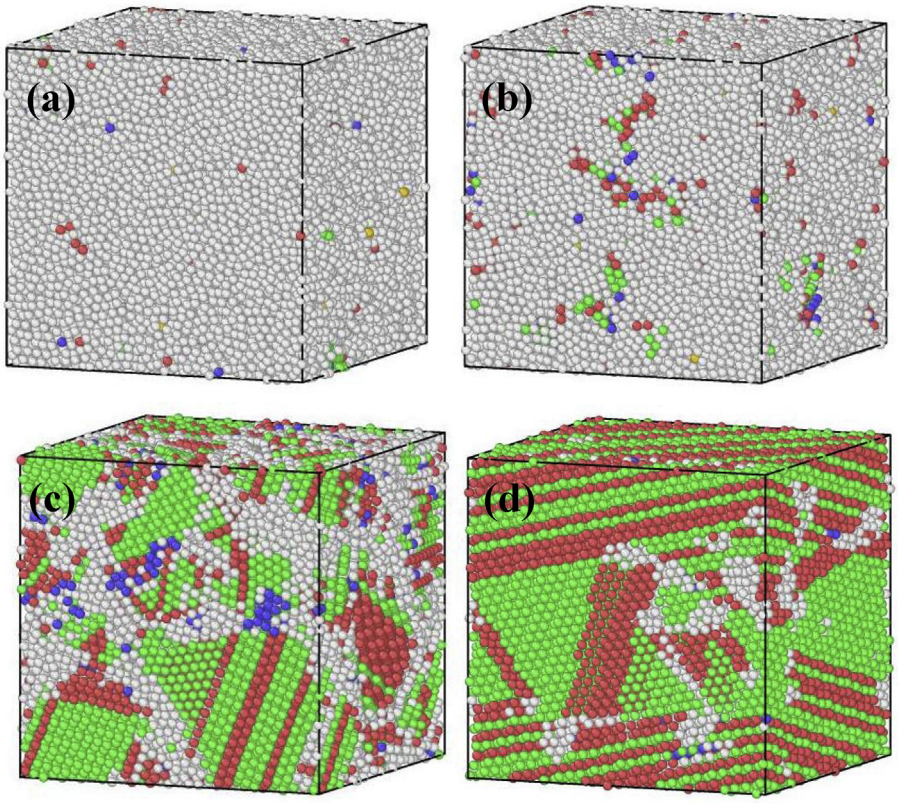

Fig. 3. Common neighbor analysis (CNA) of the quenched HEAs at 300 K at different cooling rates: (a) 5 K/ps; (b) 0.5 K/ps, (c) 0.34 K/ps and (d) 0.05 K/ps. Coloring denotes local structure: green, FCC; red, HCP; blue, BCC and white, others. (For interpretation of the references to color in this figure legend, the reader is referred to the Web version of this article.)

However, this is not the true case at Q = 0.34 K/ps and 0.05 K/ps. As shown in Fig. 5d and e, the distribution of bond pairs has been divided into two typical regions: one contains the high-symmetry 1661 bond pair; the other is comprised of the mixture of 1541 and 1441 bond pairs. The 1661 bond pairs correspond to the appearance of the HCP structure, while the 1441 bond pairs belong to a part of the FCC structure. The structural transformation and bonding characteristic of the $Al_{0.67}$CrCoCuFeNi alloy during rapid quenching can be inferred as the follows: the low-symmetry and low-coordination bond pairs, such as 1321,1431,1541 in liquid HEAs, either transform to high-symmetry and high-coordination 1551 bond pairs, or transform to 1(5,4)41 bond pairs for FCC structure and 1661 bond pairs for HCP structure, depending on the cooling rates. As the first neighbor distances of the FCC and HCP phases are identical, the HCP structure can be viewed as the precursor of the malposed FCC structure. Accordingly, if the cooling rate is low enough, we can always ultimately get to an almost single FCC structure composed of 1441 and 1541 bond pairs which transforms from the 1551 bond pairs into the intermediate metastable structures.

Table 1
Common neighbor analysis (CNA) for the quenched HEAs.

HEA	FCC	HCP	BCC	Others
Liquid	0	0	0	**100.00%**
5 K/ps	0.5%	0.8%	0.3%	**98.40%**
0.5 K/ps	2.3%	3.3%	1.1%	**93.30%**
0.34 K/ps	38.7%	28.6%	2.0%	**30.70%**
0.05 K/ps	52.2%	37.2%	0.6%	**10.00%**

4. Conclusions

In this paper, the structural and bonding transformation of the $Al_{0.67}$CrCoFeNi HEA during quenching are investigated. Some short-ranged ordered clusters are already present in the almost amorphous HEAs at a relatively high cooling rate. The atoms become packed more orderly and ultimately form a nano-polycrystalline structure dominated by FCC structures at the lowest cooling rate. The BCC and HCP structures appear only as an intermediate state

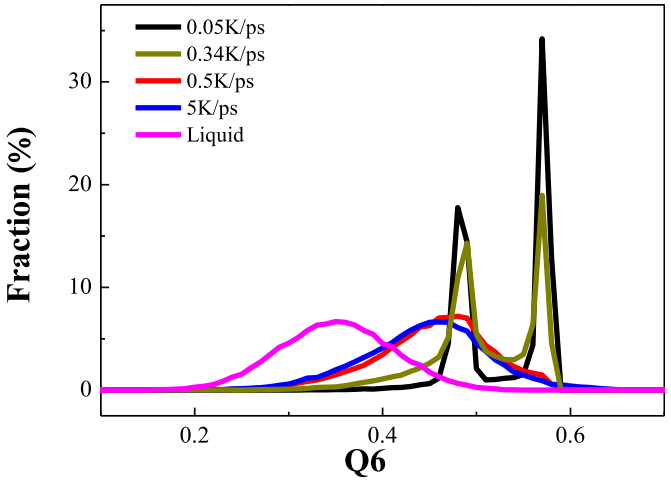

Fig. 4. Changes of the local bond orientational order parameter in the liquid and quenched states.

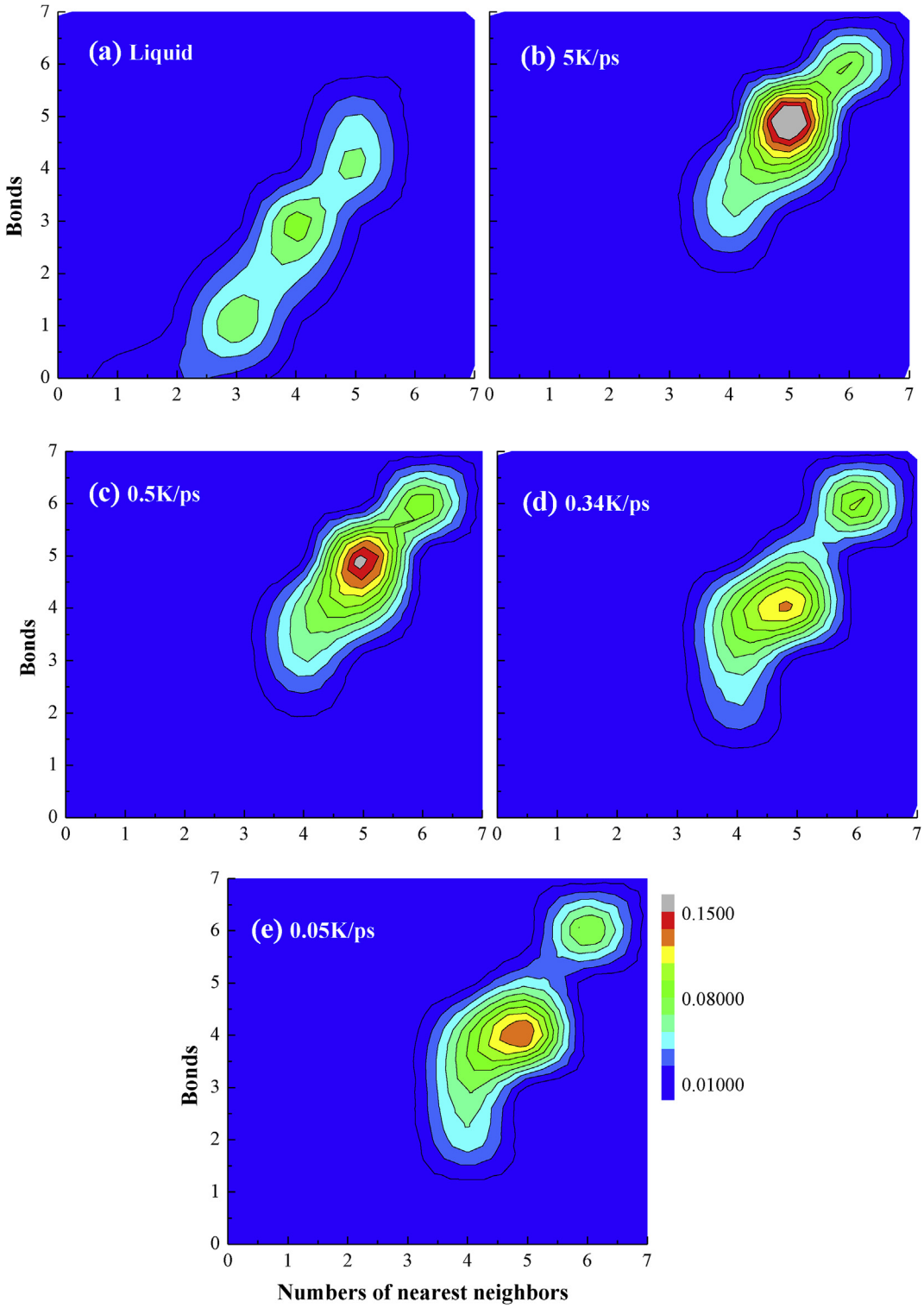

Fig. 5. Distribution of bonded pairs at different cooling rates.

acting on the course of crystallization. The cooling process can be viewed as follows: the low-symmetry and low-coordination bond pairs in the liquid HEAs, either transform to high-symmetry and high-coordination 1551 bond pairs, or transform to 1(5,4)41 bond pairs for FCC structure and 1661 bond pairs for HCP structure, depending on the cooling rates.

Acknowledgments

The authors would like to acknowledge the support by the National Natural Science Foundation of China (Grant No. 51401028, No. 51271193, No. 11402277, No. 11790292) and the Strategic Priority Research Program of the Chinese Academy of Sciences (Grant No. XDB22040303).

References

[1] Y. Zhang, T.T. Zuo, Z. Tang, M.C. Gao, K.A. Dahmen, P.K. Liaw, Z.P. Lv, Microstructures and properties of high-entropy alloys, Prog. Mater. Sci. 61 (2014) 1–93.

[2] M.H. Tsai, J.W. Yeh, High-entropy alloys: a critical review, Mater Res Lett 2 (2014) 107–123.

[3] Y.F. Ye, Q. Wang, J. Lu, C.T. Liu, Y. Yang, High-entropy alloy: challenges and prospects, Mater. Today 19 (2016) 349–362.

[4] D.B. Miracle, O.N. Senkov, A critical review of high entropy alloys and related concepts, Acta Mater. 122 (2017) 448–511.

[5] S. Singh, N. Wanderka, B.S. Murty, U. Glatzel, J. Banhart, Decomposition in multi-component AlCoCrCuFeNi high-entropy alloy, Acta Mater. 59 (2011) 182–190.

[6] T.T. Shun, Y.C. Du, Age hardening of the $Al_{0.3}CoCrFeNiC_{0.1}$ high entropy alloy, J. Alloys Compd. 478 (2009) 269–272.

[7] Z. Zhang, M.M. Mao, J. Wang, B. Gludovatz, Z. Zhang, S.X. Mao, R.O. Ritchie, Nanoscale origins of the damage tolerance of the high-entropy alloy CrMnFeCoNi, Nat. Commun. 6 (2015) 10143.

[8] C.W. Tsai, Y.L. Chen, M.H. Tsai, J.W. Yeh, T.T. Shun, S.K. Chen, Deformation and annealing behaviors of high-entropy alloy $Al_{0.5}CoCrCuFeNi$, J. Alloys Compd. 486 (2009) 427–435.

[9] L.J. Santodonato, Y. Zhang, M. Feygenson, C.M. Parish, M.C. Gao, R.J. Weber, J.C. Neuefeind, Z. Tang, P.K. Liaw, Deviation from high-entropy configurations in the atomic distributions of a multi-principal-element alloy, Nat. Commun. 6 (2015) 5964.

[10] R. Feng, M. Gao, C. Lee, M. Mathes, T. Zuo, S. Chen, J. Hawk, Y. Zhang, P. Liaw, Design of light-weight high-entropy alloys, Entropy 18 (2016) 333.

[11] H.Y. Diao, R. Feng, K.A. Dahmen, P.K. Liaw, Fundamental deformation behavior in high-entropy alloys: an overview, Curr. Opin. Solid St. M 21 (2017) 252–266.

[12] D. Ma, M. Yao, K. Pradeep, C.C. Tasan, H. Springer, D. Raabe, Phase stability of non-equiatomic CoCrFeMnNi high entropy alloys, Acta Mater. 98 (2015) 288–296.

[13] C.J. Tong, Y.L. Chen, J.W. Yeh, S.J. Lin, S.K. Chen, T Tg Shun, C.H. Tsau, S.Y. Chang, Microstructure characterization of $Al_xCoCrCuFeNi$ high-entropy alloy system with multiprincipal elements, Metall. Mater. Trans. 36 (2005) 881–893.

[14] A. Sharma, S.A. Deshmukh, P.K. Liaw, G. Balasubramanian, Crystallization kinetics in AlxCrCoFeNi ($0 \leq x \leq 40$) high-entropy alloys, Scripta Mater. 141 (2017) 54–57.

[15] Z. Li, K.G. Pradeep, Y. Deng, D. Raabe, C.C. Tasan, Metastable high-entropy dual-phase alloys overcome the strength–ductility trade-off, Nature 534 (2016) 227–230.

[16] C.C. Tasan, Y. Deng, K.G. Pradeep, M. Yao, H. Springer, D. Raabe, Composition dependence of phase stability, deformation mechanisms, and mechanical properties of the CoCrFeMnNi high-entropy alloy system, JOM 66 (2014) 1993.

[17] M. Ogura, T. Fukushima, R. Zeller, Peter H. Dederichsa, Structure of the high-entropy alloy $Al_xCrFeCoNi$: fcc versus bcc, J. Alloys Compd. 715 (2017) 454–459.

[18] C.Y. Yu, X.D. Xu, M.W. Chen, C.T. Liu, Atomistic mechanism of nano-scale phase separation in fcc-based high entropy alloys, J. Alloys Compd. 663 (2016) 340–344.

[19] A. Sharma, P. Singh, D.D. Johnson, Peter K. Liaw, G. Balasubramanian, Atomistic clustering-ordering and high-strain deformation of an $Al_{0.1}CrCoFeNi$ high-entropy alloy, Sci. Rep. 6 (2016) 31028.

[20] S. Plimpton, Fast parallel algorithms for short-range molecular dynamics, J. Comput. Phys. 117 (1995) 1–19.

[21] A. Stukowski, Extracting dislocations and non-dislocation crystal defects from atomistic simulation data, Model. Simulat. Mater. Sci. Eng. 18 (2010) 015012.

[22] L. Xie, P. Brault, A.L. Thomann, X. Yang, Y. Zhang, G.Y. Shang, Molecular dynamics simulation of Al-Co-Cr-Cu-Fe-Ni high entropy alloy thin film growth, Intermetallics 68 (2016) 78–86.

[23] L. Xie, P. Brault, A.L. Thomann, J.M. Bauchire, AlCoCrCuFeNi high entropy alloy cluster growth and annealing on silicon: a classical molecular dynamics simulation study, Appl. Surf. Sci. 285 (2013) 810–816.

[24] J.C. Huang, Evaluation of tribological behavior of Al-Co-Cr-Fe-Ni high entropy alloy using molecular dynamics simulation, Scanning 34 (2012) 325–331.

[25] K. Zhang, H. Li, L. Li, X.F. Bian, Why does the second peak of pair correlation functions split in quasi-two-dimensional disordered films? Appl. Phys. Lett. 102 (2013), 071907.

[26] H. Tsuzuki, P.S. Branicio, J.P. Rino, Structural characterization of deformed crystals by analysis of common atomic neighborhood, Comput. Phys. Commun. 177 (2007) 518–523.

[27] L. Ma, C. Li, Y. Jiang, J. Zhou, L. Wang, F. Wang, Y. Xue, J. Alloys Compd. 694 (2017) 61–67.

[28] W. Mickel, S.C. Kapfer, G.E. Schroder-Turk, K. Mecke, Shortcomings of the bond orientational order parameters for the analysis of disordered particulate matter, J. Chem. Phys. 138 (2013), 044501.

[29] K. Zhang, H. Li, Y.Y. Jiang, Liquid–liquid phase transition in quasi-two-dimensional supercooled silicon, Phys. Chem. Chem. Phys. 16 (2014) 18023–18028.

[30] J.D. Honeycutt, H.C. Andersen, Molecular dynamics study of melting and freezing of small Lennard-Jones clusters, J. Phys. Chem. 91 (1987) 4950–4963.

[31] S. Feng, L. Qi, L. Wang, S.P. Pan, M.Z. Ma, X.Y. Zhang, G. Li, R.P. Liu, Atomic structure of shear bands in $Cu_{64}Zr_{36}$ metallic glasses studied by molecular dynamics simulations, Acta Mater. 95 (2015) 236–243.

[32] S. Feng, K.C. Chan, R.P. Liu, Quantifying the microstructural inhomogeneity of Zr46Cu46Al8 metallic glasses based on change ratio of polyhedral volume, J. Alloys Compd. 731 (2018) 452–457.